

## 2-D meso-scale complex fracture modeling of concrete with embedded cohesive elements

Mingyan Shen<sup>1a</sup>, Zheng Shi<sup>1b</sup>, Chao Zhao<sup>\*1,2</sup>, Xingu Zhong<sup>1a</sup>, Bo Liu<sup>2,3a</sup> and Xiaojuan Shu<sup>1a</sup>

<sup>1</sup>Hunan Provincial Key Laboratory of Structures for Wind Resistance and Vibration Control & School of Civil Engineering,  
Hunan University of Science and Technology, Taoyuan Road, Yuhu District, Xiangtan, China

<sup>2</sup>School of Mechanics and Civil Engineering, China University of Mining and Technology (Beijing),  
Ding No.11 Xueyuan Road, Haidian District, Beijing, China

<sup>3</sup>State Key Laboratory of Deep Geomechanics and Underground Engineering, No.16 Qinghua East Road, Haidian District, Beijing, China

(Received December 19, 2018, Revised June 17, 2019, Accepted June 20, 2019)

**Abstract.** This paper has presented an effective and accurate meso-scale finite element model for simulating the fracture process of concrete under compression-shear loading. In the proposed model, concrete is parted into four important phases: aggregates, cement matrix, interfacial transition zone (ITZ), and the initial defects. Aggregate particles were modelled as randomly distributed polygons with a varying size according to the sieve curve developed by Fuller and Thompson. With regard to initial defects, only voids are considered. Cohesive elements with zero thickness are inserted into the initial mesh of cement matrix and along the interface between aggregate and cement matrix to simulate the cracking process of concrete. The constitutive model provided by ABAQUS is modified based on Wang's experiment and used to describe the failure behaviour of cohesive elements. User defined programs for aggregate delivery, cohesive element insertion and modified failure constitutive model are developed based on Python language, and embedded into the commercial FEM package ABAQUS. The effectiveness and accuracy of the proposed model are firstly identified by comparing the numerical results with the experimental ones, and then it is used to investigate the effect of meso-structure on the macro behavior of concrete. The shear strength of concrete under different pressures is also involved in this study, which could provide a reference for the macroscopic simulation of concrete component under shear force.

**Keywords:** concrete; complex fracture; meso-scale model; cohesive element; polygon aggregates

### 1. Introduction

Concrete, as a widely used construction materials, plays an indispensable role in various industrial and civil engineering constructions. For most of the current structural designs and numerical studies of large-scale concrete structures, concrete is usually regarded as a homogenous material to simplify the calculation process (Zhong *et al.* 2018, Long and Lee 2015, Sadowski *et al.* 2018, He *et al.* 2018). However, concrete is actually a multi-phase material (Contrafatto *et al.* 2016, Haeri *et al.* 2018), which is composed of four important phases: randomly-distributed aggregates, mortar, interfacial transition zone (ITZ) which is located at the interface between aggregates and cement matrix, and the initial defects (such as voids, initial cracks). The physical as well as mechanical properties of concrete greatly depend on its meso-structure. All these features lead to the randomness and heterogeneity in macro properties of concrete. Therefore, it is a vital task to quantitatively relate meso-scale information to macro properties of concrete.

Compared with time-consuming and expensive

experimental procedures, numerical modeling at the meso-scale level has shown great potential in predicting the complex nonlinear response of concrete (Zhang *et al.* 2018), in which concrete is considered as a composite material consisting of four important phases: cement matrix, aggregate, interfacial transition zone ITZs and macro-voids. However, a realistic result can be obtained only when the meso-structure of concrete is taken into account and the reasonable numerical models are developed.

Past studies (Skarzynski *et al.* 2015, Xue 2018) indicated that the macroscopic responses of concrete were significantly affected by the distribution of aggregate because the volume fraction of aggregates in usual concrete is up to 75%. The position and shape of aggregates are usually assumed to be random (Roubin *et al.* 2015), which may be the main cause of the randomness and heterogeneity in macro properties of concrete. Circle and elliptical aggregates (Luthfi *et al.* 2018, Yin *et al.* 2015) are usually used in 2D meso-scale numerical models due to the high efficiency in generation and packing of aggregates. However, a large number of research results based on image processing technology show that the aggregate in concrete are mainly random polygons with 4~10 edges (Trawinski *et al.* 2016). Therefore, the numerical model based on circle and elliptical aggregates may lead to deviations between the numerical results and the real experimental results. For the purpose of establishing the geometrical models with more

\*Corresponding author, Ph.D.

E-mail: 1020173@hnust.edu.cn

<sup>a</sup>Professor

<sup>b</sup>M.S. Student

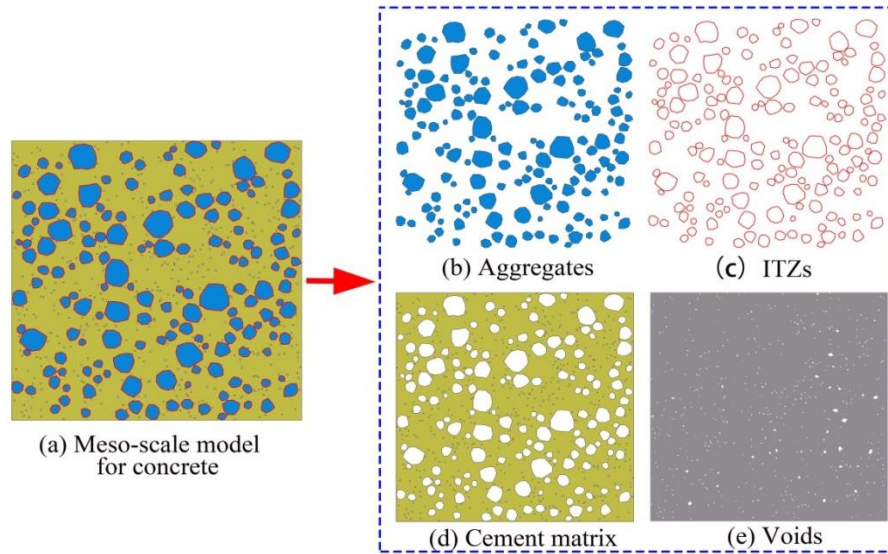


Fig. 1 (a) The meso-scale model for concrete; (b) Aggregates; (c) ITZs; (d) Cement matrix; (e) Voids

realistic aggregates, Tekin *et al.* (2018), Ren *et al.* (2015) introduced the CT scanning and 3D reconstruction techniques which are able to provide a geometrical model accurately consistent with the real concrete. Roubin *et al.* (2015) introduced the concept of random aggregate model, which means the shape, distribution and packing process of aggregates in numerical models are random. Due to the clear concept and programming convenience, the random aggregate model has been greatly enriched in recent years. Plenty of aggregates generation and packing criteria are developed, and the generation efficiency of aggregate models has been greatly improved. The shape of aggregates is becoming more diversified, from the initial circular aggregates and elliptical aggregates to the random polygonal aggregates (Chen *et al.* 2018).

During the fracture process, concrete changes from continuous medium to discontinuous one, and displacement discontinuous appear. Two types of numerical models are usually used to describe the fracture process of concrete, which are classical continuous models (Long *et al.* 2013, Bernardi *et al.* 2015, Sirico *et al.* 2017) and discrete models (Chen *et al.* 2011, Shemirani *et al.* 2018). In classical continuous models, the crack spread by changing stiffness of cracking element. These models are sensitive to the finite element mesh discretization and thus they need to be enriched with a characteristic length of micro-structure in order to provide mesh-independent results (Pijaudier-Cabot and Bazant 1987, Jirasek and Rolshoven 2003). Discrete models include lattice models (Bolander and Sukumar 2005, Kozicki and Tejchman 2007), discrete element method (Burns and Hanley 2017, Burns and Piirainen 2015), and rigid body spring models (Chen *et al.* 2018, Zhao *et al.* 2018, Zhong *et al.* 2018). These discrete models do not rely on the continuum assumption, and adjacent blocks are allowed to separate at the contact interface, which makes them convenient tools to describe the initiation and propagation of concrete cracks. Continuous model with cohesive element is another effective and efficient approach for modeling concrete fracture, especially

for uniaxial tension loading cases. This model does not need any extension, since a crack or shear zone is created in a discrete way (Morales-Alonso *et al.* 2018, Yin *et al.* 2015, AI-Osta *et al.* 2018).

ITZs are the most important component of the concrete meso-scale model, and the weakest regions of conventional concrete. Diamond *et al.* (2001) observed that the initial crack always propagate along the interface between the aggregate and the cement matrix, and the ITZs may directly affects the strength, stiffness and cracking pattern of concrete (Zhang *et al.* 2018, Zhao and Sun 2014). Therefore, the accurate understanding of the properties and behaviour of ITZs is crucial for concrete in meso-scale analyses. Existing studies (Skarzynski *et al.* 2015, Chen *et al.* 2018) have shown that the thickness of ITZ is extremely thin, which is about 50~100  $\mu\text{m}$ . It is unrealistic to consider ITZs with such a small dimension in traditional finite element models. Besides, very small elements in local region easily lead to strain localization effect, and result in unreasonable calculation results. The cohesive element model equipped with a crack initiation criterion and a traction-separation law (Yin *et al.* 2013), is an effective and efficient approach to describe the mechanical behavior of ITZs, especially in uniaxial tension loading cases. By means of meso-scale modeling with dynamically-inserted cohesive elements, Luthfi *et al.* (2018) investigated the failure mode of encapsulation-based self-healing concrete. However, the cohesive element model is only suitable for simulating mechanical tests where tensile failure is the primary focus, since it is assumed that the element only undergoes tensile failure, not shear or compression failure.

The aim of this study is to develop a more effective and accurate meso-scale finite element model with random distributed aggregates and embedded cohesive elements to analyze the complex fracture of concrete. In the proposed model, the concrete is considered as multi-phase material composed of four important phases: aggregates, cement matrix, interfacial transition zone (ITZ), and the initial defects, as shown in Fig. 1. Aggregate particles were

modelled as randomly distributed polygons with a varying diameter according to the sieve curve developed by Fuller and Thompson. Some effective methods, such as rotating the aggregate around its centroid during the packing process, have been adopted to improve the success rate of aggregate delivery. The material heterogeneity is taken into consideration by the randomness of aggregate shape and distribution. Initial defects include voids and initial cracks in concrete, but only voids are considered in this study. The voids are arbitrary polygons, and generated with the aggregates. Cohesive elements with zero thickness are inserted into the initial mesh of cement matrix and along the interface between aggregate and cement matrix to simulate the cracking process of concrete. In order to accurately describe the failure behavior of concrete, the cracking initial criterion and the traction-separation law proposed by Luthfi *et al.* (2018), Yin *et al.* (2013) are modified based on the experiment carried out by Wang *et al.* (2011), and then used to describe the failure behavior of cohesive elements. The modified constitutive model is not only suitable for concrete undergoing tensile failure, but also for concrete undergoing shear, compression and mixed failures. User defined programs for aggregate delivery, cohesive element insertion and modified fracture constitutive model has been developed based on Python language, and embedded into the commercial FEM package ABAQUS. The effectiveness and accuracy of the proposed meso-scale model are first identified by comparing the numerical results with the experimental ones, and then it is used to investigate the effect of meso-structure on the macro behavior of concrete. In additional, the shear strength of concrete under different lateral pressures is also involved in this study, which can provide a reference for the macroscopic simulation of concrete component under shear force.

The innovative points of the present research works are: 1) Aggregate particles are modeled as randomly distributed polygons with a varying diameter according to the sieve curve developed by Fuller and Thompson; 2) Cohesive elements with zero thickness are inserted into the initial mesh of cement matrix and along the interface between aggregate and cement matrix to simulate the cracking process of concrete; 3) The cracking initial criterion and the traction-separation law are modified based on the experiment results, and used to describe the failure behavior of cohesive elements; 4) Mesh sensitivity and the effect of meso-structure on the macro behavior of concrete are investigated. In additional, the shear strength of concrete under different lateral pressures is also involved in this study, which can provide a reference for the macroscopic simulation of concrete component under shear force, and the shear strength of concrete under different lateral pressures is also examined in this study.

## 2. Establishment of the aggregate model considering voids

The volume fractions of aggregates in usual concretes greatly affect the macroscopic response of concrete. Therefore, a realistic result can be obtained only when the grading, shape and distribution of aggregates in numerical

concrete are consistent with that of real concrete. In this study, an effective approach is provided to generate the geometry of aggregates. Considering that the generation of voids are similar to that of aggregates, the emphasis of this section is put on the approach of generating the geometry of aggregate.

The geometry of aggregates is generated in three steps, which are briefly documented here and then explained separately. First, determine the aggregate grading of numerical concrete by the distribution curve proposed by Fuller and Thompson; Second, generate aggregates and establish the aggregate library for numerical concrete. In order to improve the accuracy of numerical concrete, the aggregate library should accurately meet the preassigned aggregate gradation; Third, deliver aggregates into the target area and establish the geometry of aggregate models. During the delivering process, conflict judgement is carried out to ensure that adjacent aggregates are always separated from each other by a certain distance.

### 2.1 Grading of aggregate

The distribution curve proposed by Fuller and Thompson (Zhang *et al.* 2017) is used to determine the grading of aggregates

$$P'(d < d_0) = 100 \left( \frac{d_0}{d_{\max}} \right)^{0.5} \quad (1)$$

where  $P'$  is the mass percentage of aggregates that pass through the sieve diameter of  $d_0$ ,  $d_{\max}$  is the maximum diameter of aggregates.

The Fuller curve defined by Eq. (2) is mainly applicable to determine the gradation of 3-D aggregate models. In this paper, the 3D models are transformed into 2D models to improve computational efficiency, and the method proposed by Walraven (1981) is adopted to guarantee the equivalence between the 2D gradation and the 3D gradation of aggregate. According to Walraven, the mathematical formula for calculating the probability of aggregates with a diameter less than  $d_0$  is as follows

$$P(d < d_0) = P_k \left[ 1.065 \left( \frac{d_0}{d_{\max}} \right)^{0.5} - 0.053 \left( \frac{d_0}{d_{\max}} \right)^4 - 0.012 \left( \frac{d_0}{d_{\max}} \right)^6 - 0.0045 \left( \frac{d_0}{d_{\max}} \right)^8 + 0.0025 \left( \frac{d_0}{d_{\max}} \right)^{10} \right] \quad (2)$$

where  $P$  is the percentage of area occupied by aggregates that pass through the sieve diameter of  $d_0$ ;  $P_k$  is the total percentage of volume occupied by aggregates in concrete, which is taken as 0.75 in this study.

Taking usual concrete as an example, the aggregate size (diameter) are between 0~25 mm, and the volume percentage occupied by aggregates in concrete is about 75% ( $P_k = 0.75$ ). According to Eq. (2) proposed in this paper, the area percentage of aggregate used in 2D numerical model are listed in Table 1.

### 2.2 Establishment of aggregates library

Circle and elliptical aggregates are usually used in 2D

Table 1 Area percentage of aggregate for usual concrete according to Eq. (2)

Aggregate Diameter interval (mm)	0~5	5~10	10~15	15~20	20~25
Aggregate Area Ratio (%)	36	14.7	11	8.3	5

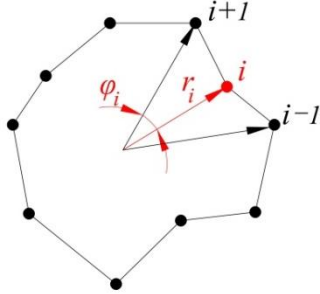


Fig. 2 Presentation of polygonal aggregates in polar coordinates

meso-scale numerical models due to the high efficiency in generation and packing of aggregates (Chen *et al.* 2018, Zhang and Wang 2018). However, a large number of research results (Trawinski *et al.* 2016, Ren *et al.* 2015) based on image processing technology show that the aggregate in concrete are mainly random polygons with 4~10 edges. Therefore, the numerical model based on circle and elliptical aggregates may lead to deviations between the numerical results and the real experimental results. In this study, an effective technique to generate arbitrary polygons (including convex and concave polygons) is provided and used to establish the aggregate library for numerical concrete.

Determining the coordinates of each vertex is the key to determine a polygon, which can be achieved by changing the polar radius  $r_i$  and the polar angle  $\varphi_i$  as shown in Fig. 2. Considering that the shape of aggregate is random, the polar radius  $r_i$  and the polar angle  $\varphi_i$  are determined by random functions

$$r_i = R_0 + (2\lambda - 1) \cdot R_f \quad (3)$$

$$\varphi_i = \frac{2\pi}{n_e} + (2\eta - 1) \cdot \frac{2\pi}{n_e} \cdot \delta \quad (4)$$

$$R_0 = (R_{\max} + R_{\min}) / 2$$

where  $\lambda$ ,  $\eta$  are random number between 0 and 1;  $R_0$  is average aggregate radius for a radius interval, and  $R_f$  is the fluctuation range for a radius interval;  $R_{\max}$ ,  $R_{\min}$  are the maximum and minimum aggregate radius of a radius interval, respectively;  $\delta$  is a constant less than 1, which defines the fluctuation degree of polar angles;  $n_e$  is the total number of convexes in a polygon. Eq. (3) shows that the polar radiuses of polygon vertexes range from  $R_0 - R_f$  to  $R_0 + R_f$ , and Eq. (4) indicates that the polar angles corresponding to each vertex range from  $2\pi(1 - \delta)/n_e$  to  $2\pi(1 + \delta)/n_e$ .

In order to improve the accuracy of numerical simulation, the aggregate library or the aggregate model

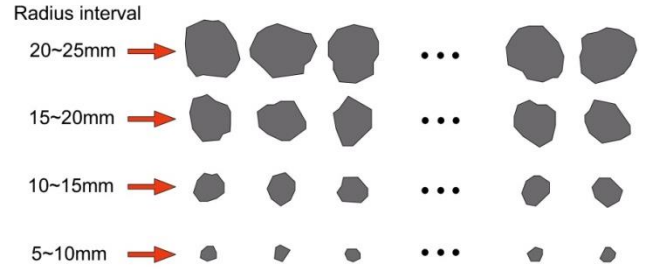


Fig. 3 Computer-generated sections of aggregate with different average radius

should accurately meet the preassigned aggregate gradation. In this study, a new method is presented to establish the aggregate library, which is more accurate and convenient. There are two key steps should be noted in the proposed method: First, once an aggregate is generated, its area should be calculated and then add it to the total aggregate area of current radius interval; Second, when inequality (5) is satisfied, which means that the accumulative area of packed aggregates is very close to the preassigned aggregate area  $A_{interval}$ , stop generating new aggregates of current radius interval, and calculate the residual area  $\Delta A$  of current radius interval according to Eq. (6). After that, turn to next radius interval and repeat the previous steps until the aggregate library meets the assigned aggregate gradation. It should be noted that the residual area  $\Delta A$  of current radius interval is to be considered in the next radius interval. Fig. 3 provides an example of the aggregate library generated proposed method.

$$\sum_{i=1}^k A_i + \pi R_0^2 > A_{interval} \quad (5)$$

( $k$  is the number of aggregate packed)

$$\Delta A = A_{interval} - \sum_{i=1}^k A_i \quad (6)$$

### 2.3 Packing process of aggregates

The packing process of aggregates is carried out by determining the centroid of aggregates. The distribution of aggregate is random in real concrete, so the packing process of aggregates is also a stochastic process. In order to increase the success rate of aggregate packing, two key points should be paid more attention. Firstly, aggregate should be packed from ones with large sizes to those with small sizes according to aggregate radius intervals; Secondly, when a new aggregate conflict with the existing aggregate, rotates the aggregate around its centroid, as shown in Fig. 4.

In real concrete, aggregates are always separated from each other by a certain distance, and there are no overlaps or conflicts. But for numerical concrete, conflicts between adjacent aggregates are unavoidable during the packing process. Therefore, it is necessary to carry out conflict judgment. In this paper, an effective conflict judgment method is presented to judge whether an aggregate conflicts

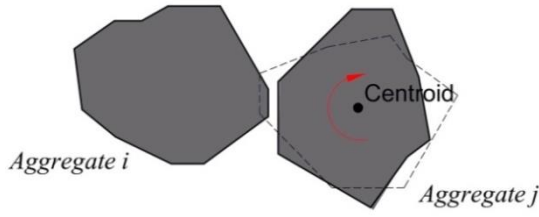


Fig. 4 Rotating the aggregate around its centroid

with other aggregates. This method is applicable to aggregate with arbitrary shape, including convex polygons and concave polygons. Generally speaking, the vertex of one aggregate is inside the other aggregate when two aggregates conflict, which can be identified by ray method. Making a ray from target point (the vertex of an aggregate), then check the number of intersections between the ray and edges of a polygonal aggregate. If the number of intersection points is odd, the target point is inside the aggregate, e.g., the point *i* in Fig. 5; Otherwise, the target point is outside the aggregate, e.g., the point *j* in Fig. 5. It should be noted that polygon nodes must be stored in sequence, which is a prerequisite to carry out the conflict judgment.

In order to improve the efficiency of conflict judgment, an additional judgment process based on Eq. (7) is added. If Eq. (7) is satisfied, it means there is a far distance and no conflicts between the two aggregates; Otherwise, the two aggregates may overlap, and conflict judgment is carried out.

$$O_1O_2 > (D_{1max} + D_{2max})/2 \tag{7}$$

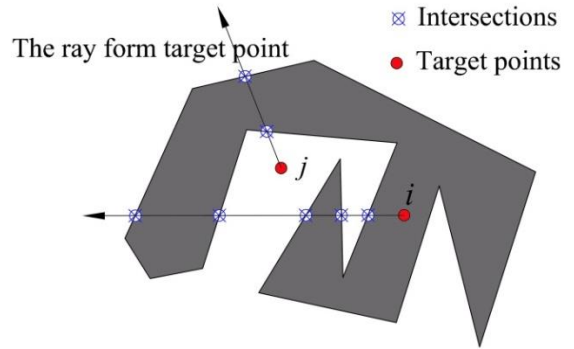


Fig. 5 The method to determine a point in or outside a aggregate

where  $O_1O_2$  is the centroid distance between aggregate 1 and aggregate 2;  $D_{1max}$ ,  $D_{2max}$  are the maximum aggregate radius of aggregate 1 and aggregate 2, which are defined according to the radius interval of the two aggregate, respectively.

User defined programs based on Python language and ABAQUS software are developed and used to establish the aggregate model. The flow chart for generating aggregate model is shown in Fig. 6, and Fig. 7 provides an aggregate model established by the proposed program. The adopted specimen is rectangular (400 mm×400 mm) and the aggregate radius ranges from 0 to 25 mm. The area percentage of aggregate in concrete are determined by Eq. (2) and listed in Table 1. The statistics data of the aggregate model are shown in Table 2, which indicates that the aggregate model is able to meet the preassigned aggregate gradation accurately, and the proposed program is efficient.

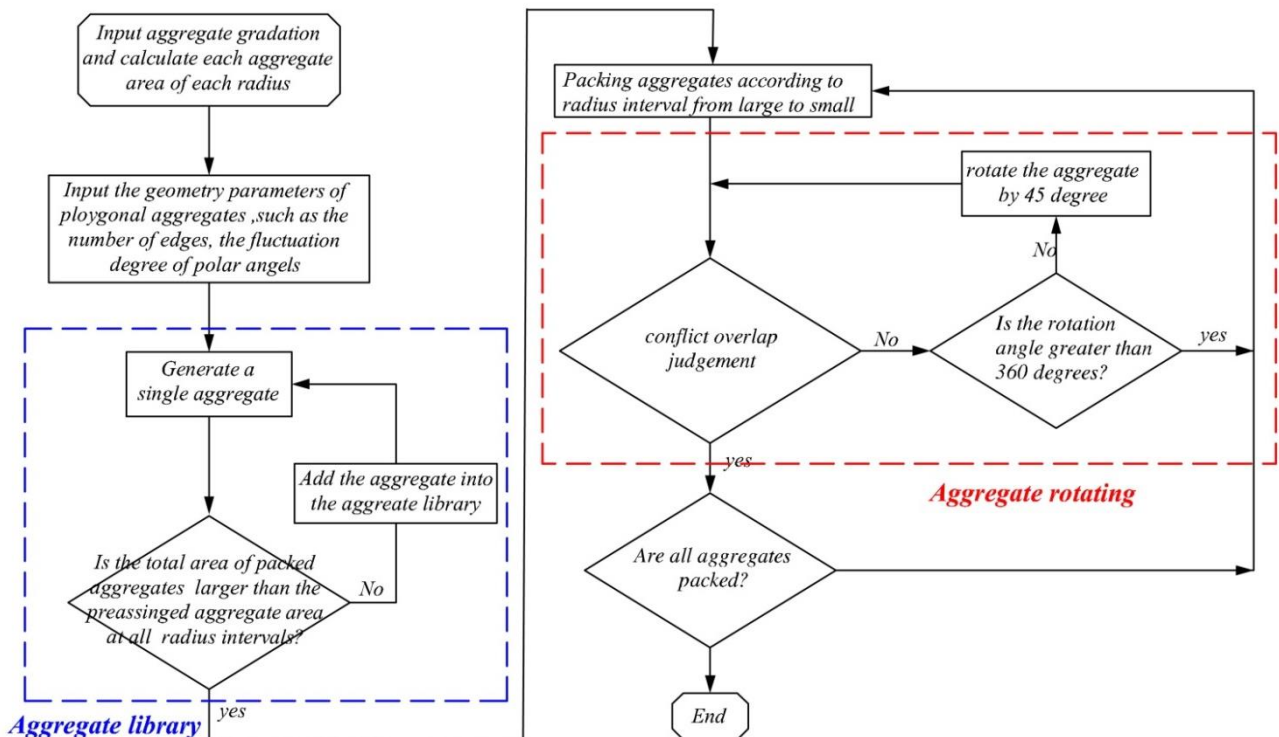


Fig. 6 Aggregate packing process proposed in this study

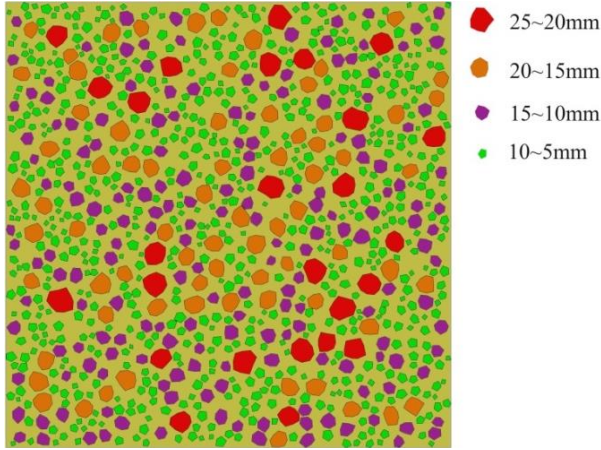


Fig. 7 A aggregate model established by user defined programs

Table 2 Statistics date of aggregate model established by the proposed program

Radius interval	Preassigned aggregate gradation			Numerical results		
	Mass percentage	Aggregate area (mm <sup>2</sup> )	Area percentage (2D)	Aggregate area (mm <sup>2</sup> )	Area percentage	Number of aggregates
25~20 (mm)	10.56%	7957.55	4.97%	7957.55	4.97%	26
20~15 (mm)	11.98%	13111.31	8.19%	13111.31	8.19%	73
15~10 (mm)	14.21%	17432.48	10.90%	17432.43	10.90%	182
10~5 (mm)	18.52%	23515.04	14.70%	23515.01	14.70%	700
<5 (mm)	44.73%	57983.62	36.24%	/	/	/

\* Mass percentage and area percentage (2D) is determined by Eqs. (1) and (2), respectively; Aggregates (<5 mm) are ignored in numerical model.

### 3. Application of cohesive elements in the meso-scale concrete model

Existing researches (Diamond *et al.* 2011, Zhang *et al.* 2018) indicate that cracks always occur in the cement matrix of concrete, or propagate along the interface between the aggregate and the cement matrix. In order to simulate the fracture process of concrete, cohesive elements are introduced and inserted into the initial mesh of cement matrix and along ITZs of the numerical model in this paper.

In this section, the basic principle of the cohesive element is briefly described, and then we mainly focus on the fracture constitutive model for the cohesive element.

#### 3.1 Cohesive elements

Cohesive elements are inserted into the initial mesh of FEMs, each cohesive element has two interface (upper and lower interfaces), which connected by a pair of uniformly distributed springs as shown in Fig. 8.

The displacement of the cohesive element is determined by the relative displacement of upper interface and lower interface. The stiffnesses of the uniformly distributed springs are related to the mechanical properties of ITZs.

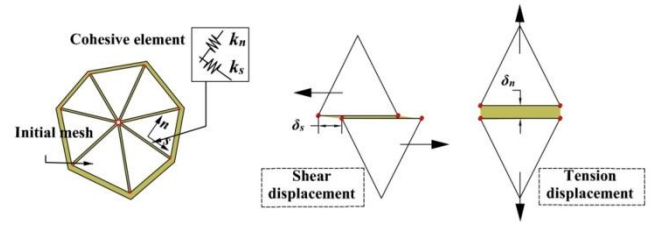


Fig. 8 Cohesive elements

The element stress  $\mathbf{T}$  are expressed as follows

$$\mathbf{T} = [\sigma_n \quad \sigma_s]^T = \mathbf{D}\boldsymbol{\delta}$$

$$\mathbf{D} = \begin{bmatrix} k_n & \\ & k_s \end{bmatrix} \quad \boldsymbol{\delta} = [\delta_n \quad \delta_s] \quad (8)$$

where  $\sigma_n$ ,  $\sigma_s$  denote the normal and tangential stress of the cohesive element, respectively;  $\mathbf{D}$  is the matrix of interfacial spring stiffness, which is defined by the normal spring  $k_n$  and the tangential spring  $k_s$ ;  $\boldsymbol{\delta}$  is the displacement of the cohesive element, which consist of two components, normal displacement  $\delta_n$  and the tangential displacement  $\delta_s$ .

#### 3.2 Fracture constitutive model for cohesive elements

In a 2D scenario, three fracture modes can be simulated by the cohesive element: the opening mode (Mode I), the shearing mode (Mode II), and the mixed mode (Mode I-II). Considering that the first two modes are special of the mixed mode, the focus of this section is put on the mixed mode. The failure constitutive model usually consists of two components: damage initiation and damage evolution. Therefore, the description of fracture constitutive model for cohesive elements in this paper is carried out with the two aspects.

##### 3.2.1 Damage initiation of cohesive elements

Damage initiation defines a critical value, and the stiffness of the material begins to weaken when the critical value is reached. The damage initiation criterion proposed by Zhao *et al.* (2014), Luthfi *et al.* (2018), which is only focus on the effect of tension on shear strength, is expressed as follows

$$\left\{ \frac{\langle \sigma_n \rangle}{\sigma_n^0} \right\}^2 + \left\{ \frac{\sigma_s}{\sigma_s^0} \right\}^2 = 1 \quad (9)$$

$$\langle \sigma_n \rangle = \begin{cases} 0 & \sigma_n \leq 0 \\ \sigma_n & \sigma_n > 0 \end{cases} \quad (10)$$

where  $\sigma_n^0$ ,  $\sigma_s^0$  is the tensile strength and shear strength of cohesive element, respectively;  $\sigma_n$ ,  $\sigma_s$  are the normal and tangential stress of the cohesive element defined in Eq. (8);  $\sigma_n^0$ ,  $\sigma_s^0$  are positive when the cohesive element in the tensile state;  $\sigma_s^0$  and  $\sigma_s$  are always positive.

According to Wang *et al.* (2011), the shear strength of ITZs is closely related to the compressive stress perpendicular to the interface. Therefore, the above damage

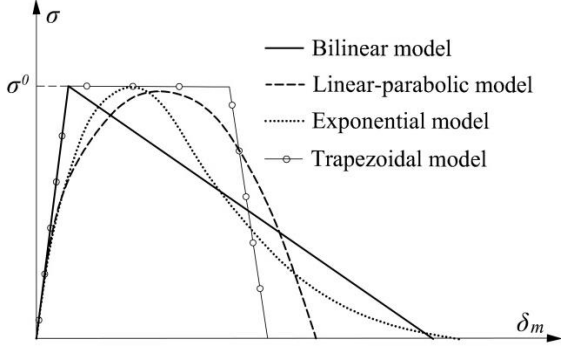


Fig. 9 Damage constitutive models for cohesive element

initiation criterion is modified based on Wang's experiment in this study, and the effect of compressive stress on shear stress is considered as follows

$$\left\{ \frac{\sigma_s}{\sigma_s^0} \right\}^2 = 1 \quad (\sigma_n \leq 0) \quad (11)$$

$$\sigma_s^0 = \begin{cases} 0.102 f_m - \tan 35^\circ \cdot \sigma_n & (0.6 f_m \leq \sigma_n < 0) \\ 1.305 f_m + 1.305 \cdot \sigma_n & (f_m < \sigma_n < 0.6 f_m) \end{cases} \quad (12)$$

where  $f_m$  is the axial compressive strength of cement matrix.

### 3.2.2 Damage evolution of cohesive elements

Damage evolution describes the degradation process of mechanical properties after reaching the critical value of damage initiation, which is defined by introducing a stiffness damage factor  $\omega$  in this study. The factor  $\omega$  varies from 0 (no damage) to 1 (complete damage). For reducing the analysis complexity, it supposes that the normal stiffness  $k_n$  and the tangential spring  $k_s$  are weakened by the same damage factor. Correspondingly, the stiffness of the damaged interface element is expressed as follows

$$\begin{aligned} k_n &= k_n^0 (1 - \omega) \\ k_s &= k_s^0 (1 - \omega) \end{aligned} \quad (\sigma_n \leq 0) \quad (13)$$

where  $k_n^0$ ,  $k_s^0$  is the initial stiffness of materials.

The above equation indicates that determining the damage factor  $\omega$  is the key to describe the damage evolution of materials. For cohesive elements, there are several constitutive models which have been adopted (Alfano 2006), as shown in Fig. 9.

By comparing the accuracy and efficiency of different methods, bilinear model is adopted in this paper, and the damage factor  $\omega$  is obtained by the following formula

$$\omega = \frac{\delta_m^f (\delta_m - \delta_m^0)}{\delta_m (\delta_m^f - \delta_m^0)} \quad (14)$$

where  $\delta_m$  is the opening displacement for the mixed fracture mode of cohesive elements, determined by the normal displacement  $\delta_n$  and the tangential displacement  $\delta_s$ .

$$\delta_m = \sqrt{(\delta_n)^2 + (\delta_s)^2} \quad (15)$$

$\delta_m^0$  is the opening displacement corresponding to the damage initiation. In this study,  $\delta_m^0$  is determined by the following formula according to Luthfi *et al.* (2018)

$$\delta_m^0 = \sqrt{1 + \beta^2} \frac{\sigma_n^0 \sigma_s^0}{\sqrt{k_n^2 (\sigma_s^0)^2 + k_s^2 (\sigma_n^0)^2}} \quad \beta = \frac{\delta_s}{\delta_n} \quad (16)$$

$\delta_m^f$  is the opening displacement for  $\omega=1$ , which reflects the fracture energy release rate of materials under complex stress state. The determination of  $\delta_m^f$  is based on Benzeggagh-Kenane (BK) law (Kou *et al.* 2011), and it supposes that the normal stiffness  $k_n$  and the tangential spring  $k_s$  are weakened by the same damage factor in order to reduce the analysis complexity. The formula of  $\delta_m^f$  is as follows

$$\delta_m^f = 2\sqrt{1 + \beta^2} \frac{G_{IC} + (G_{IIC} - G_{IC}) \left( \frac{\lambda}{1 + \lambda} \right)^\eta}{(1 + \lambda) \frac{\sigma_n^0 \sigma_s^0}{\sqrt{(\sigma_s^0)^2 + \kappa^2 (\sigma_n^0)^2}}} \quad (17)$$

$$\kappa = \frac{\sigma_s}{\sigma_n} = \frac{k_s^0 \beta}{k_n^0} \quad \lambda = \frac{G_{II}}{G_I} = \frac{k_s^0 \beta^2}{k_n^0} \quad (18)$$

$G_{IC}$  and  $G_{IIC}$  are the fracture toughness for mode I and mode II, which mean the amount of energy consumed to create a crack of one unit area.  $G_I$  and  $G_{II}$  are the cohesive fracture energy for mode I and mode II;  $\eta$  is a constant of materials, which is set to 0.3 according to Kou *et al.* (2011).

## 4. Presentation of studied cases

To verify the accuracy of the proposed method and investigate the nonlinear behaviors of concrete, a double-notched concrete specimen proposed by Nooru-Mohamed (1992) is studied. Geometry, loading and supporting arrangements of the tested specimen are shown in Fig. 10. The thickness of the plate is 50 mm. Gravel is adopted in the concrete, and details about the aggregate gradation are listed in Table 3. There are two complex fracture modes mentioned in Nooru-Mohamed's experiment: tension-shear fracture mode and compression-shear fracture mode. In tension-shear fracture, the specimen is firstly loaded by the shear load  $P_s = 10$  kN. Subsequently, it continues keeping the applied shear force  $P_s$  constant, and progressively increasing the axial vertical force  $P_n$  until the specimen is broken down. In compression-shear fracture, the specimen is firstly loaded by the axial compression force  $P_n = -1$  kN. Subsequently, it continues keeping the applied compression force  $P_n$  constant, and progressively increasing the shear force  $P_s$  until the specimen is broken down. Fracture modes of the tested specimen under different loading conditions are shown in Fig. 11. The relationship between applied forces and corresponding displacement are recorded during the loading process, and

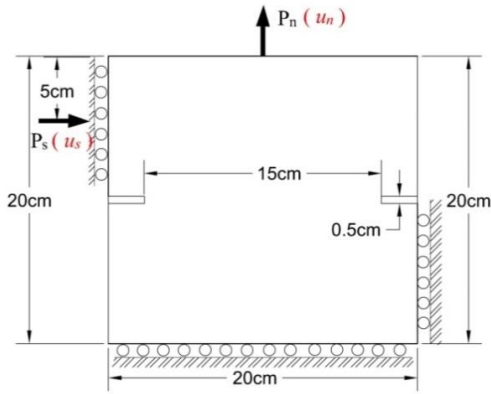


Fig. 10 the tested specimen

Table 3 Aggregate gradation of concrete in Nooru-Mohammed's experiment

Radius interval (mm)	0.0~1.0	1.0~2.0	2.0~4.0	4.0~8.0	8.0~16.0
Aggregates (kg/m <sup>3</sup> )	293	458	256	365	457
Portland cement (kg/m <sup>3</sup> )			375		
water (kg/m <sup>3</sup> )			187.5		

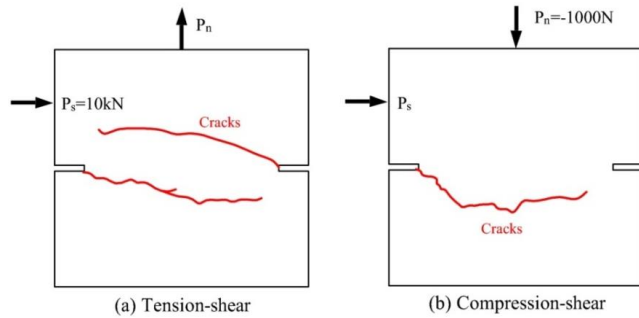


Fig. 11 Fracture mode of the tested specimen

compared with numerical results in following sections.

#### 4.1 Effectiveness of the proposed fracture constitutive model

In order to identify the performance of the proposed fracture constitutive model in fracture analysis of concrete, the numerical model of the double-notched concrete specimen is developed, as shown in Fig. 12. Triangular elements are adopted to simulate the aggregate and cement matrix, and the average size of triangular elements is 1.5 mm. In order to describe the cracking behavior of cement matrix and simulate the mechanical behavior of ITZs, cohesive elements are inserted into the initial mesh of cement matrix and along the interface between aggregate and cement matrix. Two loading conditions consistent with that of Nooru-Mohamed's experiments, namely the compression loading condition and the tension shear condition, are investigated. Numerical models based on the modified fracture constitutive model and the original constitutive model defined by ABAQUS are developed and compared to identify the validity and accuracy of the proposed constitutive model. Material properties of

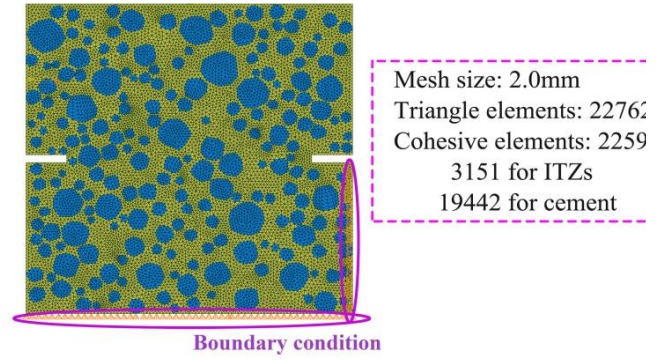


Fig. 12 Meso-scale model for the double-notched concrete specimen in Nooru-Mohammed's experiment

Table 4 Material properties in the meso-scale model of concrete

	Bulk elements		Cohesive elements	
	Aggregate	Cement matrix	Cement matrix	ITZs
$E$ [GPa]	70.0	25.0	-	-
$\nu$	0.2	0.2	-	-
$k_n^0$ [MPa/mm]	-	-	$10^9$	$10^9$
$k_s^0$ [MPa/mm]	-	-	$10^9$	$10^9$
$\sigma_n^0$ [MPa]	-	-	4	2
$G_{Ic}$ [N/m]	-	-	40	20
$G_{IIc}$ [N/m]	-	-	400	200
$f_m$ [MPa]	-	-	49.66	-

\*Aggregate smaller than 2 mm are considered as ingredients of the mastic in this study;  $G_{Ic}$ ,  $G_{IIc}$ ,  $k_n^0$  and  $k_s^0$  are determined according to Luthfi *et al.* (2018), López *et al.* (2008).

concrete are shown in Table 4.

Figs. 13 and 14 present the stress contour plots (according to traditional FEM elements, not cohesive elements) and cracking process predicted by different numerical models. It is seen in Fig. 13 that the elements around cracks are in compression-shear state in compression-shear loading, and the stress (including shear stress and principle stress) and crack propagation predicted by the modified constitutive model in which the effect of compressive stress on shear strength is considered, are obviously higher than that predicted by the original constitutive model in which the effect of compressive stress on shear strength is neglected. In tension-shear loading condition, the elements around cracks are mainly in tension-shear state, as shown in Fig. 14, and the stress (including shear stress and principle stress) and the crack propagation predicted by the modified constitutive model is consistent with that predicted by the original constitutive model in the whole loading process. The load-displacement curves under different loading conditions and with different constitutive models are presented and compared with experimental results in Fig. 15. It is seen that the load-displacement curve predicted by the modified constitutive model is in good agreement with the experiment results, not only under the tension-shear loading condition, but also under the compression-shear loading condition, while the ultimate

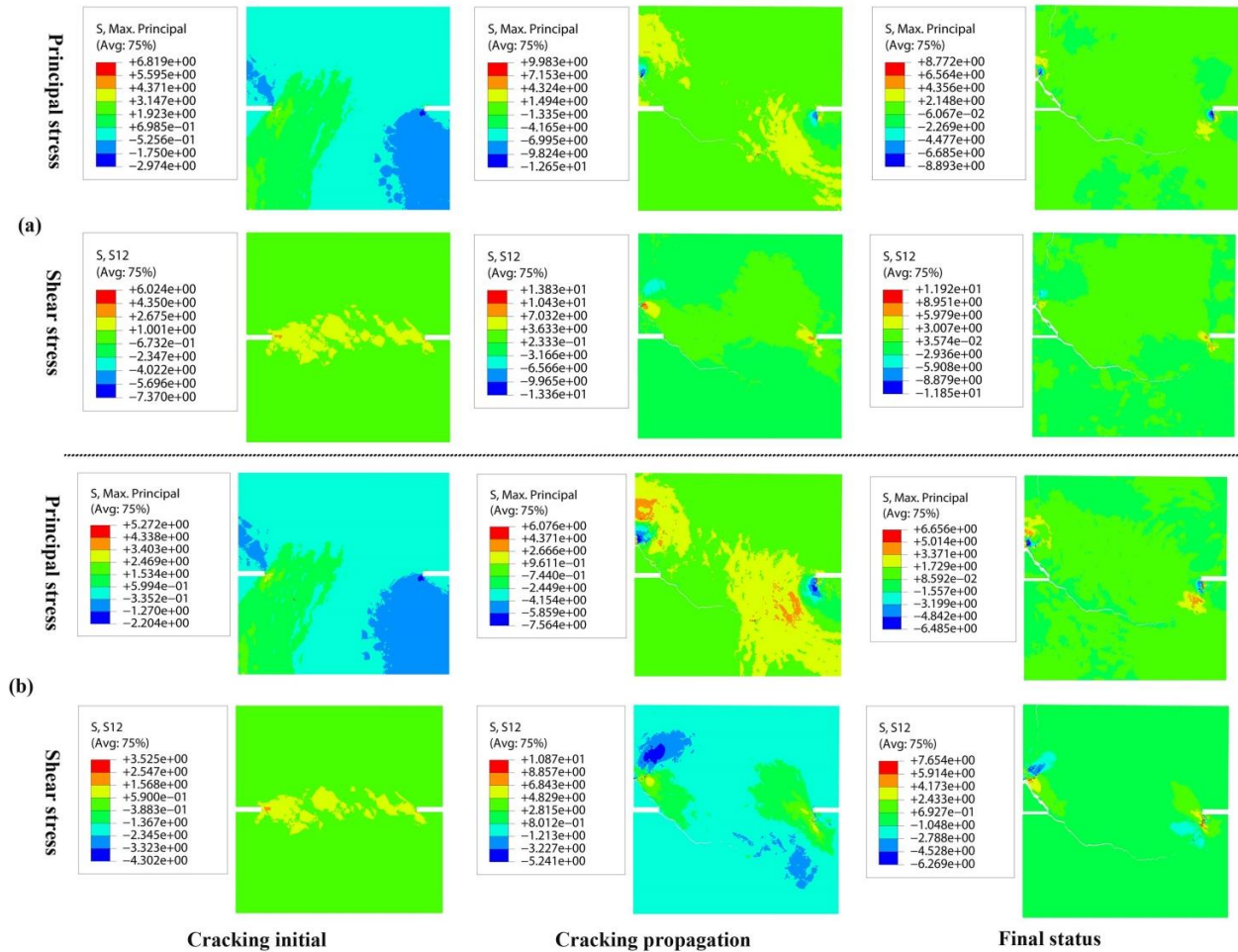


Fig. 13 Stress contour plots from numerical models under compression-shear loading (a) the modified constitutive model; (b) the original constitutive model provided by ABAQUS

shear strength predicted by the original constitutive model is obviously lower than that from results from the experiment tests and the numerical model with modified constitutive model. Generally, the modified constitutive model proposed in the study is not only suitable for concrete undergoing tensile shear failure, but also for concrete undergoing compression shear failures, while the original is only suitable for concrete undergoing tensile shear failure.

#### 4.2 Mesh sensitive analysis of meso-scale models

In the proposed model, cracks in concrete can only propagate along the cohesive elements inserted. Therefore, the mesh size and the interface orientation may affect the numerical results. In order to clarify the influence of element grid on numerical results, four comparative numerical models with different global size (1.5 mm, 2.5 mm, 5 mm and 10 mm) are developed, as shown in Fig. 16(a). Material properties adopted in numerical models are shown in Table 4, and only the tension-shear loading condition is investigated. The cracking modes of different models are listed in Fig. 16(b). We divide all orientations into 36 sections from  $0^\circ$  to  $180^\circ$  with the increment of  $5^\circ$ ,

and count the number of interfaces (or cohesive elements) lying in each section as shown in Fig. 16(c), which are helpful for us to understand the influence of interface orientations on numerical results. The load-displacement curves are plotted and compared with experimental results in Fig. 17.

According to Fig. 17, the curves from numerical models with global size (1.5 mm and 2.5 mm) are closer to experimental results, while the ultimate strength from numerical model with global size (5 mm and 10 mm) are higher than experimental results. Considering the computational efficiency and accuracy of numerical models, the optimal global size in this study is 2.5 mm, which is approximately between  $R_{\min}/2$  and  $R_{\min}$  ( $R_{\min}$  is the radius of the smallest aggregate). In addition, the distribution of interface orientation gets more isotropic with the increase of element number, as shown in Fig. 16, and the numerical results are more consistent with the experimental ones.

#### 4.3 Influence of aggregate shape and distribution

Three comparative numerical models with the same aggregate gradation and different aggregate shape (polygon,

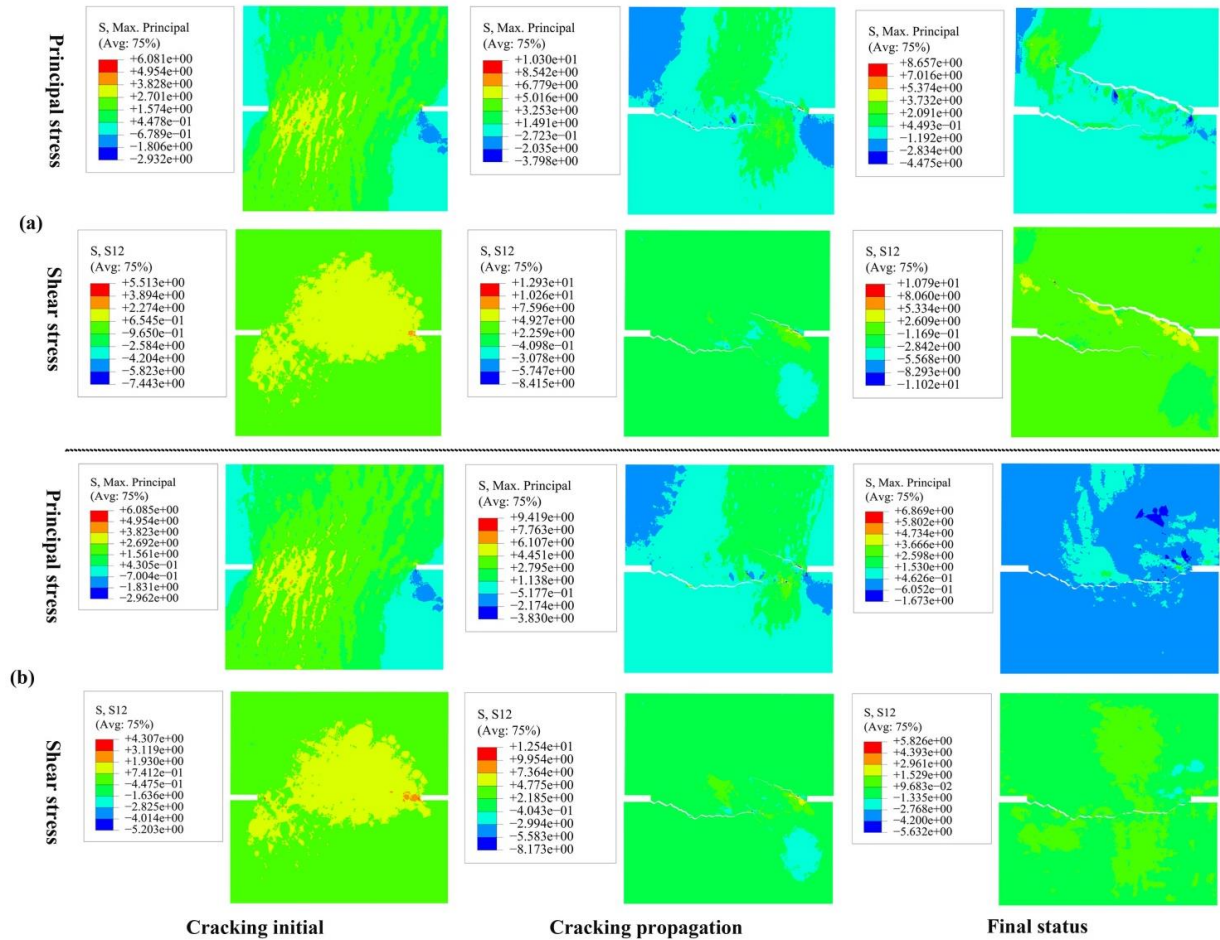


Fig. 14 Stress contour plots from numerical models under tension-shear loading (a) the modified constitutive model; (b) the original constitutive model provided by ABAQUS

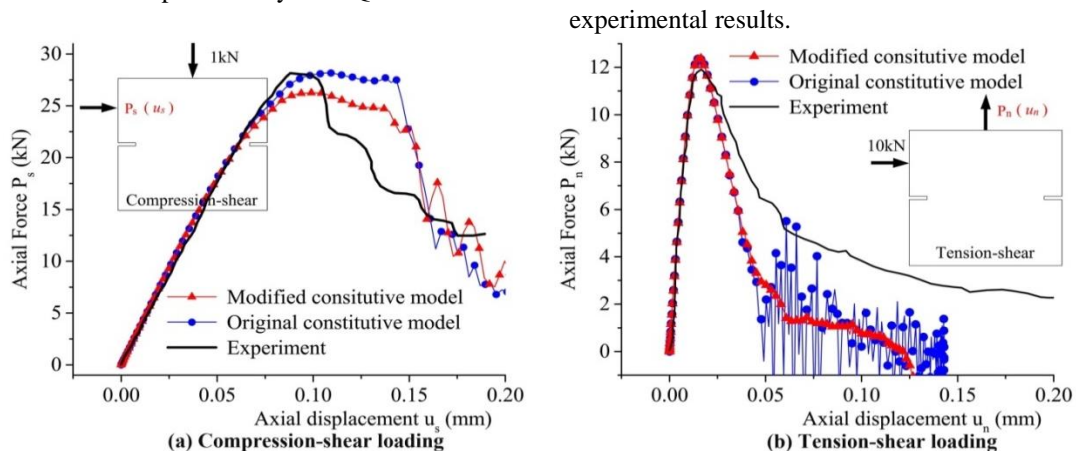


Fig. 15 Load-displacement curves predicted by numerical models under different loading conditions

ellipse and circle) are developed to investigate the influence of aggregate shape and distribution on the numerical results. Material properties adopted in numerical models are shown in Table 4, and only the tension-shear loading condition is investigated. Figs. 18-19 present the cracking modes and load-displacement curves predicted by different numerical models. Results indicate that aggregate shape has obvious influence on cracking paths and load-displacement curves of the specimen, and the results predicted by the numerical model with polygon aggregates are more close to the

#### 4.4 Influence of aggregate gradation

To investigate the influence of aggregate gradation on macro mechanical behavior of concrete, four comparative numerical models with same area percentage of aggregates ( $P_k=0.75$ ) and different aggregate gradation (the maximum aggregate sizes  $R_{max} = 10, 16, 32$  and 40) are developed. Material properties adopted in numerical models are shown in Table 4, and only the tension-shear loading condition is investigated. Fig. 20 presents the fracture mode and load-

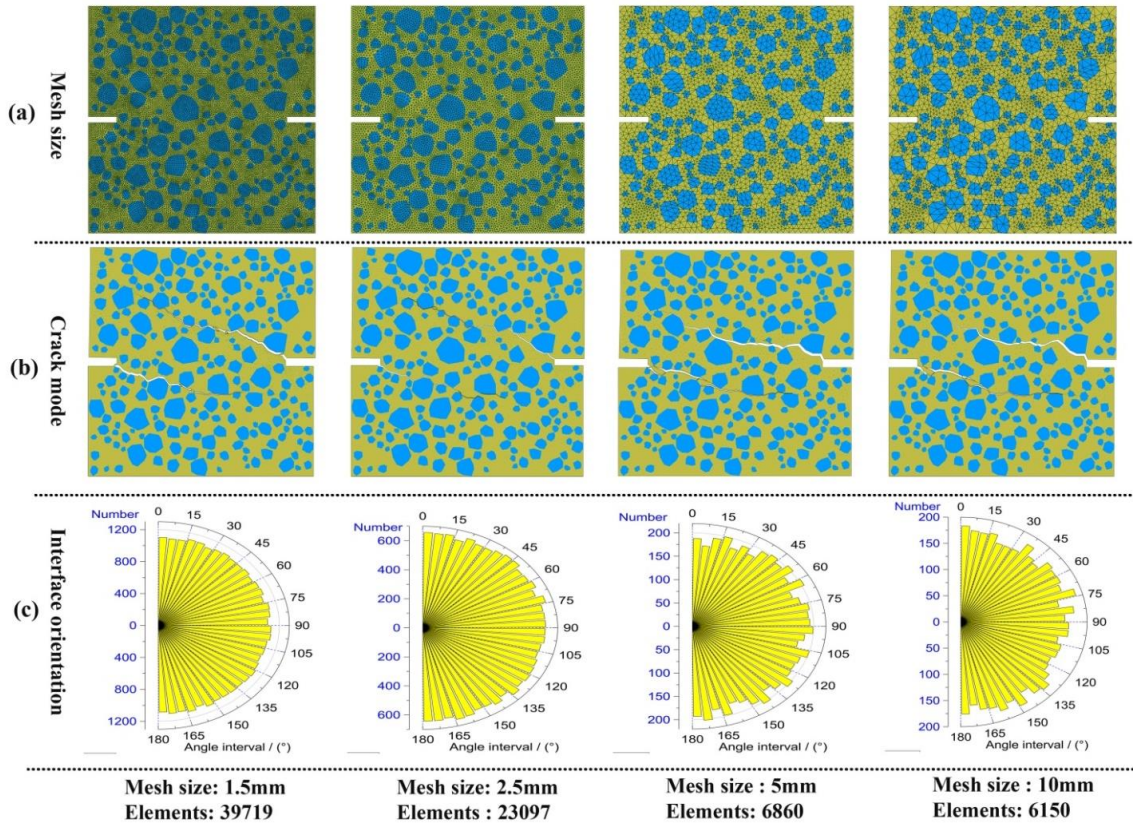


Fig. 16 (a) Meso-scale models with different mesh sizes; (b) The crack modes predicted by different models; (c) Interface orientation distribution of different models

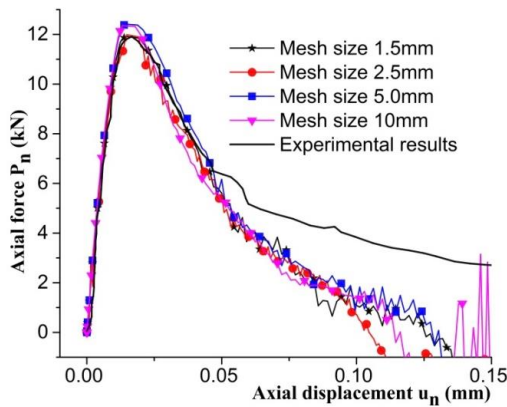


Fig. 17 Load ( $P_n$ ) - displacement ( $u_n$ ) curves predicted by numerical models with different mesh sizes

displacement curves predicted by different numerical models, which indicates that aggregate gradations have obvious influence on cracking paths and load-displacement curves of the tested specimen. In addition, with the increase of aggregate radiuses, ultimate strength of concrete under tension-shear loading condition increases.

#### 4.5 Influence of voids on the mechanical behavior of concrete

According to Li *et al.* (2018), the voids occupy 2% of concrete volume, and the diameters of voids range from 0.5~1.5 mm, which is another key factor affecting the

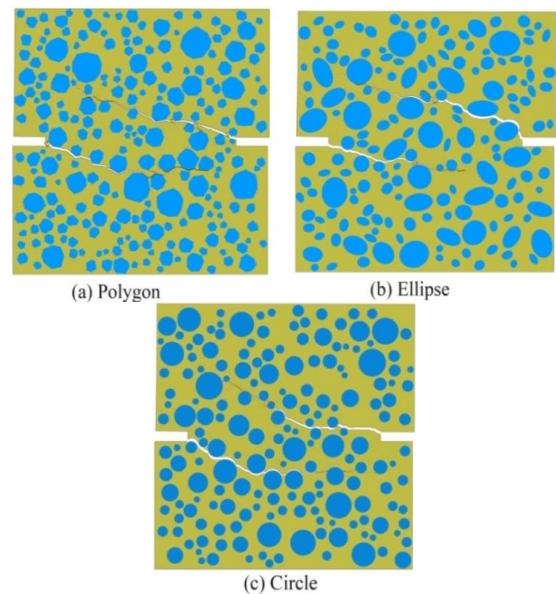


Fig. 18 Fracture mode predicted by numerical models with different aggregate shapes

macro mechanical behavior of concrete. In order to clarify the influence of voids, four comparative numerical models with different voids ratio (0, 1%, 2% and 3%) are developed. Material properties adopted in numerical models are shown in Table 4, and only the tension-shear loading condition is investigated. Figs. 21-22 present the fracture modes and load-displacement curves predicted by different

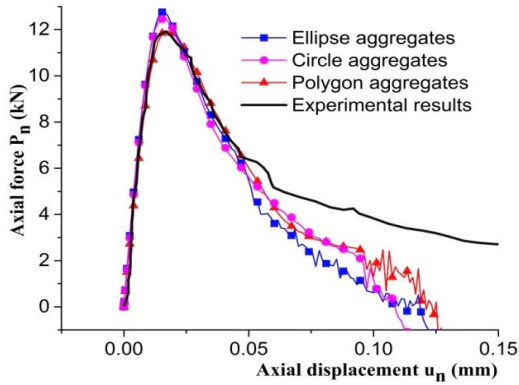


Fig. 19 Load ( $P_n$ ) - displacement ( $u_n$ ) curves from numerical models with different aggregate shapes

numerical models. It is shown that voids in concrete have obvious influence on cracking paths and load-displacement curves of the specimen. With the increase of void ratios, ultimate strength of concrete under tension-shear loading condition decreases.

4.6 Shear strength of concrete under different pressures

In practice engineering, there are a large number of concrete members under compression-shear loading, i.e., the prestressed concrete beams and tunnel lining. The pressure applied on concrete members can greatly improve the shear strength of concrete, which is always neglected in practice designs and numerical analyses due to lack of experimental data. In this section, the shear properties of concrete under different pressures are investigated based on the proposed numerical model. The target specimen is shown in Fig. 23, and the material properties adopted are listed in Table 4. The specimen is firstly loaded by the axial stress  $\sigma_n = 2, 1.5, 1, 0.5, 0, -0.5, -1.0, -1.5, -2.0, -2.5, -3.0, -4.0$ MPa. Subsequently, it continues keeping the applied axial stress  $\sigma_n$  constant, and progressively increasing the shear force  $P_s$  until the specimen is broken down. The

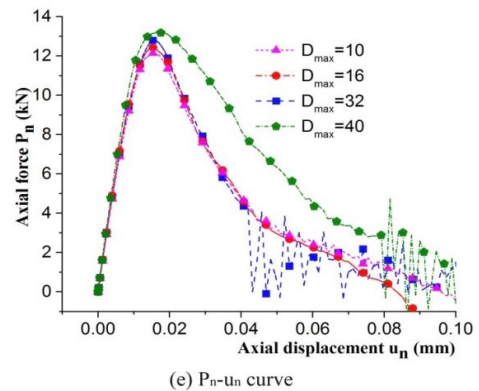
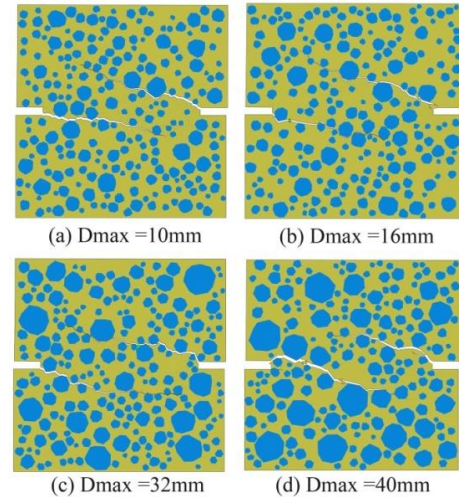


Fig. 20 Fracture mode predicted by numerical models with different aggregate radiuses

relationship between the shear force  $P_s$  and the corresponding displacement  $u_s$  is plotted in Fig. 24(a), and the relationship between the shear strength  $\tau_s$  and the axial stress  $\sigma_n$ , are shown in Fig. 24(b). Fracture modes predicted by numerical models under different loading conditions are shown in Fig. 25. It can be found that the shear strength  $\tau_s$  of concrete, which is greatly influenced

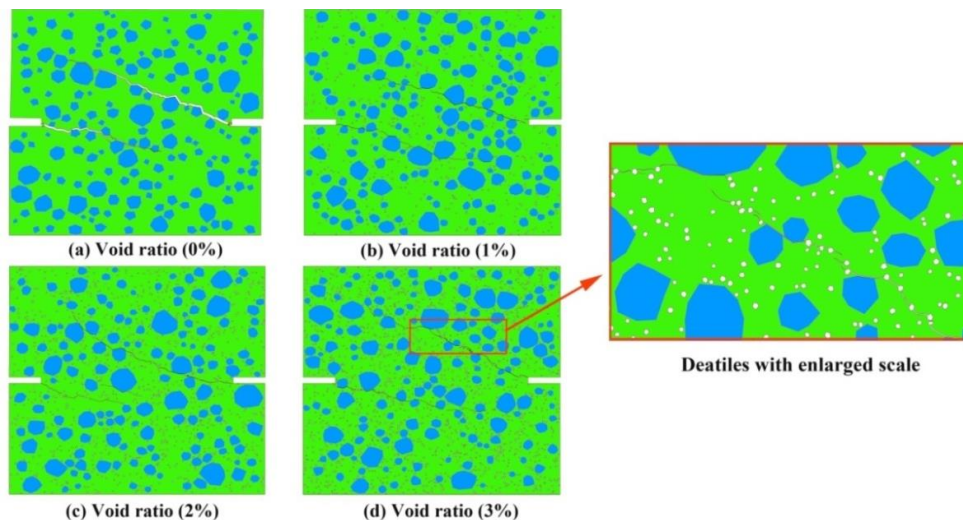


Fig. 21 Fracture mode predicted by numerical models with different void ratios

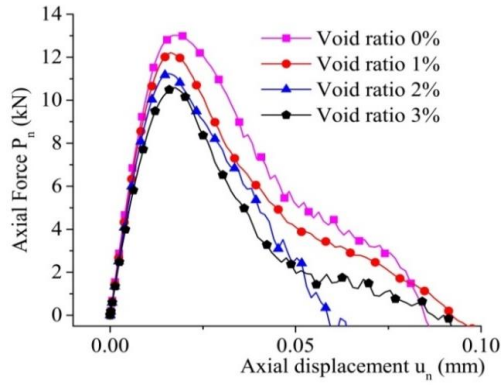


Fig. 22 Load ( $P_s$ )-displacement ( $u_n$ ) curves from numerical models with different void ratios

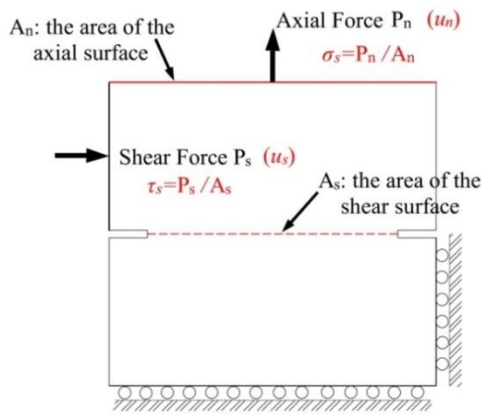
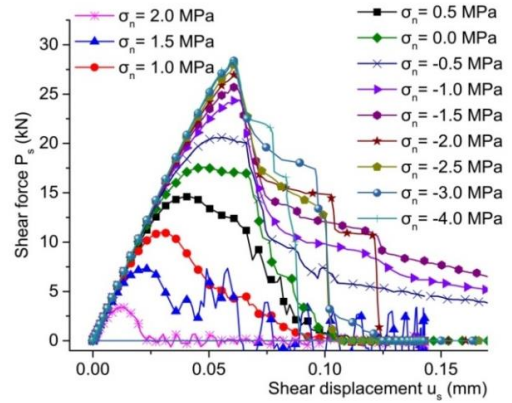
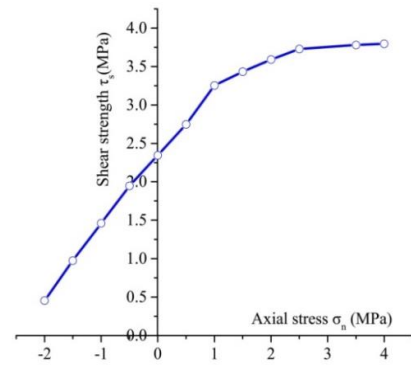


Fig. 23 Details of Loading conditions during the shear strength analyses



(a)



(b)

Fig. 24 (a) Load ( $P_s$ )-displacement ( $u_n$ ) curves from numerical models under different pressures; (b) Relationship between the shear strength  $\tau_s$  and the axial stress  $\sigma_n$

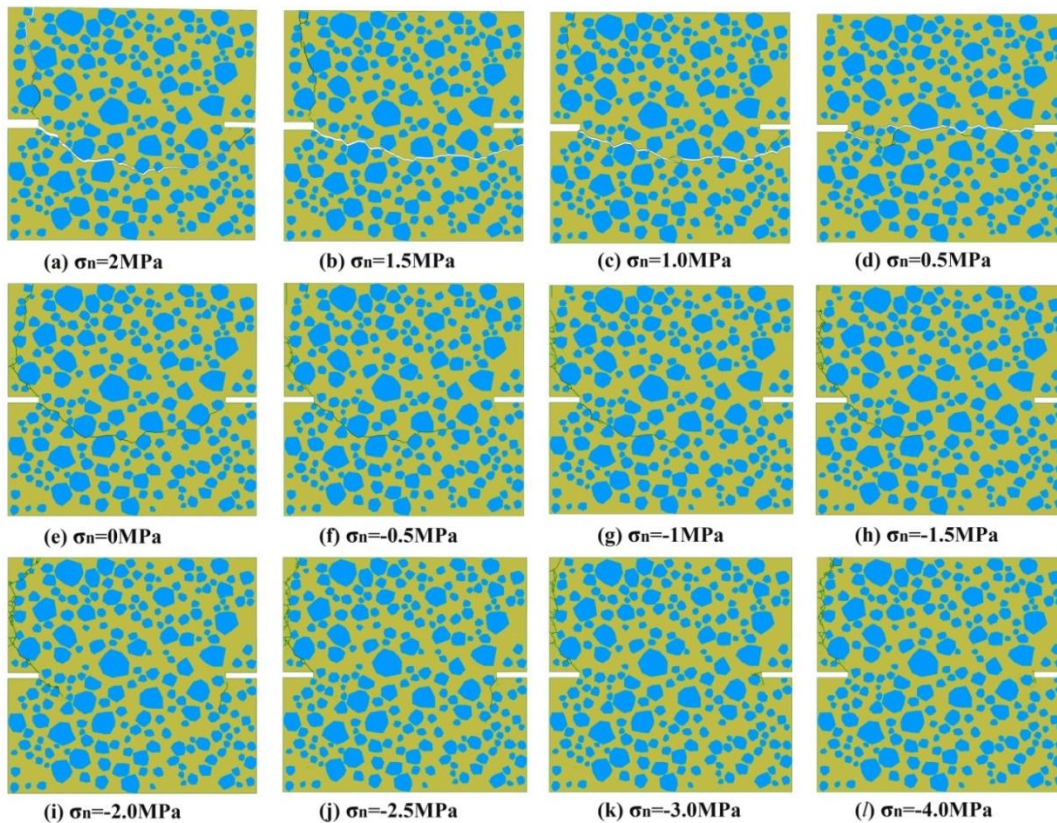


Fig. 25 Fracture modes predicted by numerical models under different loading conditions

by axial stress, increases with the increase of axial pressure stress  $\sigma_n$ . However, there is an upper limit of 3.6 MPa for the shear strength.

## 5. Conclusions

This paper has presented an effective and accurate meso-scale finite element model for simulating the fracture process of concrete under tension-shear loading and compression-shear loading. User defined programs for aggregate delivery, cohesive element insertion and modified fracture constitutive model are developed based on Python language, and embedded into the commercial FEM package ABAQUS. The effectiveness and accuracy and efficiency of the proposed meso-scale model are firstly identified by comparing the numerical results with the experimental ones, and then it is used to investigate the effect of meso-structure on the macro behavior of concrete. In addition, the shear strength of concrete under different pressures is also involved in this study. According to the results of this research, the following conclusions are drawn:

- The proposed meso-scale model with random distributed aggregates and embedded cohesive elements, is an effective and accurate meso-scale finite element model for simulating the complex fracture of concrete, and could successfully predict the load-deformation response, ultimate strengths, failure mechanisms, and cracking patterns of concrete material.
- The proposed algorithm to establish aggregate model of concrete is efficient and accurate. It considers the material heterogeneity by the randomness of aggregate shape and distribution, and is able to accurately meet the perpassaged aggregate gradation with high efficiency. In addition, the success rate of aggregate delivery is also improved by introducing some effective methods, such as rotating the aggregate around its centroid during the packing process. User defined programs based on Python language are developed and embedded into the commercial FEM package ABAQUS, which makes it convenient and efficient to establish a meso-scale model for concrete.
- Considering that the original constitutive model provided by ABAQUS is only suitable for tension-shear failure, a modified constitutive model based on the experiment results is proposed for cohesive elements in this study. The proposed model is not only suitable for concrete undergoing tensile shear failure, but also for concrete undergoing compression shear failures. Based on the model, the effect of compressive stress on the shear strength of concrete is investigated, and a relationship model between the shear strength  $\tau_s$  and the axial stress  $\sigma_n$  is established, which can provide reference for the shear design and similar numerical analyses of concrete members.
- The effect of mesh sensitivity and meso-structure on macro behavior of concrete is investigated. The results show that the mesh size and the interface orientation has some influence on the numerical results, and the optimal global size of the mesh grid is approximately between

$R_{\min}/2$  and  $R_{\min}$ , where  $R_{\min}$  refers to the smallest aggregate radius; Aggregate gradation, shape and void ratio greatly affect the macro behavior of concrete. In addition, the shear strength of concrete under different lateral pressures is also investigated by the proposed meso-scale model, and the shear strength  $\tau_s$  of concrete increases with the increase of axial stress  $\sigma_n$ . However, there is an upper limit of shear strength for the selected concrete.

## Acknowledgments

The research described in this paper is financially supported by the Natural Science Foundation of China (51678253, 41472259) and National Key Research and Develop Program of China (2016YFC080250504). These supports are gratefully acknowledged.

## References

- Alfano, G. (2006), "On the influence of the shape of the interface law on the application of cohesive-zone models", *Compos. Sci. Technol.*, **66**, 723-730. <https://doi.org/10.1016/j.compscitech.2004.12.024>.
- Al-Osta, M.A., Al-Sakkaf, H.A., Sharif, A.M., Ahmad, S. and Baluch, M.H. (2018), "Finite element modelling of corroded RC beams using cohesive surface bonding approach", *Comput. Concrete*, **22**(2), 167-182. <https://doi.org/10.12989/cac.2018.22.2.167>.
- Bernardi, P., Cerioni, R. and Michelini, E. (2015), "Numerical modelling of the cracking behaviour of RC and SFRC shear-critical beams", *Eng. Fract. Mech.*, **167**, 151-166. <https://doi.org/10.1016/j.engfracmech.2016.04.008>.
- Bolander, J.E. and Sukumar, N. (2005), "Irregular lattice model for quasistatic crack propagation", *Phys. Rev. B*, **59**, 1-20. <https://doi.org/10.1103/PhysRevB.71.094106>.
- Burns, S.J. and Hanley, K.J. (2017), "Establishing stable time-steps for DEM simulations of non-collinear planar collisions with linear contact laws", *Int. J. Numer. Meth. Eng.*, **110**, 186-200. <https://doi.org/10.1002/nme.5361>.
- Burns, S.J. and Piiroinen P.T. (2015), "Simulation and long-term behaviour of unconstrained planar rigid bodies with impact and friction", *Int. J. Nonlin. Mech.*, **77**, 312-324.
- Chen, H., Xu, B., Mo, Y.L. and Zhou, T. (2018), "Behaviour of meso-scale heterogeneous concrete under uniaxial tensile and compressive loadings", *Constr. Build. Mater.*, **178**, 418-431. <https://doi.org/10.1016/j.conbuildmat.2018.05.052>.
- Chen, J., Pan, T.Y. and Huang, X.M. (2011), "Discrete element modelling of asphalt concrete cracking using a user-defined three-dimensional micromechanical approach", *J. Wuhan Univ. Technol.-Mater. Sci. Ed.*, **26**(6), 1215-1221. <https://doi.org/10.1007/s11595-011-0393-z>.
- Chen, J.Y., Zhang, W.P. and Gu, X.L. (2018), "Mesoscale model for cracking of concrete cover induced by reinforcement corrosion", *Comput. Concrete*, **22**(1), 53-62. <https://doi.org/10.12989/cac.2018.22.1.053>.
- Contrafatto, L., Cuomo, M. and Gazzo, S. (2016), "A concrete homogenisation technique at meso-scale level accounting for damaging behaviour of cement paste and aggregates", *Comput. Struct.*, **173**, 1-18. <https://doi.org/10.1016/j.compstruc.2016.05.009>.
- Diamod, S. and Huang, J.D. (2001), "The ITZ in concrete: A different view based on image analysis and SEM observations",

- Cement Concrete Compos.*, **23**(2), 179-188. [https://doi.org/10.1016/S0958-9465\(00\)00065-2](https://doi.org/10.1016/S0958-9465(00)00065-2).
- Haeri, H., Sarfarazi, V., Zhu, Z. and Marji, M.F. (2018), "Simulating the influence of pore shape on the Brazilian tensile strength of concrete specimens using PFC2D", *Comput. Concrete*, **22**(5), 469-479. <https://doi.org/10.12989/cac.2018.22.5.469>.
- He, J., Pan, F., Cai, C.S., Habte, F. and Chowdhury, A. (2018), "Finite-element modelling framework for predicting realistic responses of light-frame low-rise buildings under wind loads", *Eng. Struct.*, **164**, 53-69. <https://doi.org/10.1016/j.engstruct.2018.01.034>.
- Jirasek, M. and Rolshoven, S. (2003), "Comparison of integral-type nonlocal plasticity models for strain-softening materials", *Int. J. Eng. Sci.*, **41**, 1553-1602. [https://doi.org/10.1016/S0020-7225\(03\)00027-2](https://doi.org/10.1016/S0020-7225(03)00027-2).
- Kou, J.F., Xu, F., Guo, J.P. and Xu, Q. (2011), "Damage laws of cohesive zone model and selection of Parameters", *J. Mech. Strength*, **33**(5), 714-718. (In Chinese)
- Kozicki, J. and Tejchman, J. (2007), "Effect of aggregate structure on fracture process in concrete using 2D lattice model", *Arch. Mech.*, **59**(4), 365-384.
- Li, D., Li, Z., Lv, C., Zhang, G. and Yin, Y. (2018), "A predictive model of the effective tensile and compressive strengths of concrete considering porosity and pore size", *Constr. Build. Mater.*, **170**, 520-526. <https://doi.org/10.1016/j.conbuildmat.2018.03.028>.
- Li, D., Li, Z., Lv, C., Zhang, G. and Yin, Y. (2018), "A predictive model of the effective tensile and compressive strengths of concrete considering porosity and pore size", *Constr. Build. Mater.*, **170**, 520-526. <https://doi.org/10.1016/j.conbuildmat.2018.03.028>.
- Long, X. and Lee, C.K. (2015), "Improved strut-and-tie method for 2D RC beam-column joints under monotonic loading", *Comput. Concrete*, **15**(5), 807-831. <https://doi.org/10.12989/cac.2015.15.5.807>.
- Long, X., Bao, J.Q., Tan, K.H. and Lee, C.K. (2014), "Numerical simulation of reinforced concrete beam/column failure considering normal-shear stress interaction", *Eng. Struct.*, **74**, 32-43. <https://doi.org/10.1016/j.engstruct.2014.05.011>.
- López, C.M., Carol, I. and Aguado, A. (2008), "Meso-structural study of concrete fracture using interface elements. II: compression, biaxial and Brazilian test", *Mater. Struct.*, **41**, 601-620. <https://doi.org/10.1617/s11527-007-9312-3>.
- Luthfi M.M., Zhuang, X.Y. and Rabczuk, T. (2018), "Computational modelling of fracture in encapsulation-based self-healing concrete using cohesive elements", *Compos. Struct.*, **196**, 63-75. <https://doi.org/10.1016/j.compstruct.2018.04.066>.
- Morales-Alonso, G., Rey-de-Pedraza, V., Gálvez, F. and Cendón, D.A. (2018), "Numerical simulation of fracture of concrete at different loading rates by using the cohesive crack model", *Theor. Appl. Fract. Mech.*, **96**, 308-325. <https://doi.org/10.1016/j.tafmec.2018.05.003>.
- Nooru-Mohamed, M.B. (1992), "Mixed mode fracture of concrete: an experimental approach", Ph.D Thesis, TU Delft, The Netherlands.
- Pijaudier-Cabot, G. and Bazant, Z.P. (1987), "Nonlocal damage theory", *ASCE J. Eng. Mech.*, **113**, 1512-1533. [https://doi.org/10.1061/\(ASCE\)0733-9399\(1987\)113:10\(1512\)](https://doi.org/10.1061/(ASCE)0733-9399(1987)113:10(1512)).
- Ren, W., Yang, Z., Sharma, R., Zhang, C.H. and Withers, P.J. (2015), "Two-dimensional X-ray CT image based meso-scale fracture modelling of concrete", *Eng. Fract. Mech.*, **133**, 24-39. <https://doi.org/10.1016/j.engfracmech.2014.10.016>.
- Roubin, E., Colliat, J.B. and Benkemoun, N. (2015), "Meso-scale modelling of concrete: A morphological description based on excursion sets of random fields", *Comput. Mater. Sci.*, **102**, 183-195. <https://doi.org/10.1016/j.commatsci.2015.02.039>.
- Sadowski, L., Nikoo, M. and Nikoo, M. (2018), "Concrete compressive strength prediction using the imperialist competitive algorithm", *Comput. Concrete*, **22**(4), 355-363. <https://doi.org/10.12989/cac.2018.22.4.355>.
- Shemirani, A.B., Sarfarazi, V., Haeri, H. and Marji, M.F. (2018), "A discrete element simulation of a punch-through shear test to investigate the confining pressure effects on the shear behaviour of concrete cracks", *Comput. Concrete*, **21**(2), 189-197. <https://doi.org/10.12989/cac.2018.21.2.189>.
- Sirico, A., Michelini, E., Bernardi, P. and Cerioni, R. (2017), "Simulation of the response of shrunk reinforced concrete elements subjected to short-term loading: a bi-dimensional numerical approach", *Eng. Fract. Mech.*, **174**, 64-79. <https://doi.org/10.1016/j.engfracmech.2016.11.020>.
- Skarzynski, L., Nitka, M. and Tejchman, J. (2015), "Modelling of concrete fracture at aggregate level using FEM and DEM based on X-ray  $\mu$ CT images of internal structure", *Eng. Fract. Mech.*, **147**, 13-35. <https://doi.org/10.1016/j.engfracmech.2015.08.010>.
- Tekin, I., Birgul, R. and Aruntas, H.Y. (2018), "X-ray CT monitoring of macro void development in mortars exposed to sulphate attack", *Comput. Concrete*, **21**(4), 367-376. <https://doi.org/10.12989/cac.2018.21.4.367>.
- Trawinski, W., Bohinski, J. and Tejchman, J. (2016), "Two-dimensional simulations of concrete fracture at aggregate level with cohesive elements based on X-ray  $\mu$ CT images", *Eng. Fract. Mech.*, **168**, 204-226. <https://doi.org/10.1016/j.engfracmech.2016.09.012>.
- Walraven, J. and Reinhardt, H. (1981), "Theory and experiments on the mechanical behaviour of cracks in plain and reinforced concretes subjected to shear loading", *Herony*, **26**, 26-33.
- Wang, Z.L., Gu, X.L. and Lin, F. (2011), "Experimental study on failure criterion of mortar under combined stresses", *J. Build. Mater.*, **4**(4), 235-245. (In Chinese)
- Xue, X.H. (2018), "Evaluation of concrete compressive strength based on an improved PSO-LSSVM model", *Comput. Concrete*, **21**(5), 505-511. <https://doi.org/10.12989/cac.2018.21.5.505>.
- Yin, A., Yang, X., Zeng, G. and Gao, H. (2015), "Experimental and numerical investigation of fracture behaviour of asphalt mixture under direct shear loading", *Constr. Build. Mater.*, **86**, 21-32. <https://doi.org/10.1016/j.conbuildmat.2015.03.099>.
- Yin, A., Yang, X., Zhang, C., Zeng, G. and Yang, Z. (2015), "Three-dimensional heterogeneous fracture simulation of asphalt mixture under uniaxial tension with cohesive crack model", *Constr. Build. Mater.*, **76**, 103-117. <https://doi.org/10.1016/j.conbuildmat.2014.11.065>.
- Yin, A.Y., Yang, X.H. and Yang, Z.J. (2013), "2D and 3D fracture modelling of asphalt mixture with randomly distributed aggregates and embedded cohesive cracks", *Constr. Build. Mater.*, **76**, 103-117. <https://doi.org/10.1016/j.piutam.2013.01.013>.
- Zhang, J., Wang, Z., Yang, H., Wang, Z. and Shu, X. (2018), "3D meso-scale modelling of reinforcement concrete with high volume fraction of randomly distributed aggregates", *Constr. Build. Mater.*, **164**, 350-361. <https://doi.org/10.1016/j.conbuildmat.2017.12.229>.
- Zhang, S., Zhang, C., Liao, L. and Wang, C. (2018), "Numerical study of the effect of ITZ on the failure behaviour of concrete by using particle element modelling", *Constr. Build. Mater.*, **170**, 776-789. <https://doi.org/10.1016/j.conbuildmat.2018.03.040>.
- Zhang, Z., Song, X., Liu, Y., Wu, D. and Song, C. (2017), "Three-dimensional mesoscale modelling of concrete composites by using random walking algorithm", *Compos. Sci. Technol.*, **149**, 235-245. <https://doi.org/10.1016/j.compscitech.2017.06.015>.
- Zhao, C., Zhong, X., Liu, B., Shu, X. and Shen, M. (2018), "A modified RBSM for simulating the failure process of RC

- structures”, *Comput. Concrete*, **21**(2), 219-229.  
<https://doi.org/10.12989/cac.2018.21.2.219>.
- Zhao, Q., Lisjak, A., Mahabadi, O., Liu, Q. and Grasselli, G. (2014), “Numerical simulation of hydraulic fracturing and associated microseismicity using finite-discrete element method”, *J. Rock Mech. Geotech. Eng.*, **6**, 574-581.  
<https://doi.org/10.1016/j.jrmge.2014.10.003>.
- Zhao, S. and Sun, W. (2014), “Nano-mechanical behaviour of a green ultra-high performance concrete”, *Constr. Build. Mater.*, **63**(7), 150-160.  
<https://doi.org/10.1016/j.conbuildmat.2014.04.029>.
- Zhong, X., Peng, X., Yan, S., Shen, M. and Zhai, Y. (2018), “Assessment of the feasibility of detecting concrete cracks in images acquired by unmanned aerial vehicles”, *Auto. Constr.*, **89**, 49-57. <https://doi.org/10.1016/j.autcon.2018.01.005>.
- Zhong, X., Zhao, C., Liu, B., Shu, X. and Shen, M. (2018), “A 3-D RBMSM for simulating the failure process of RC structures”, *Struct. Eng. Mech.*, **65**(3), 291-302.  
<https://doi.org/10.12989/sem.2018.65.3.291>.